

Detection and Classification of RBCs and WBCs in Urine Analysis with Deep Network

Xingguo Zhang, Guoyue Chen, Kazuki Saruta and Yuki Terata

Faculty of Systems Science and Technology

Akita Prefectural University

Akita, Japan

e-mail: {xingguozhang, chen, saruta, terata}@akita-pu.ac.jp

Abstract—Urinary sediment examination is used to evaluate the possible urinary tract diseases of patients. Currently, numerous approaches are applied to automatically detect Red Blood Cells (RBCs) and White Blood Cells (WBCs) from urinary sediment images. However, it is still a challenging task due to the cellular heterogeneity. Deep learning approaches have been shown to produce encouraging results on image detection in various tasks. In this paper, we investigate issues involving Faster Regions with Convolutional Neural Network (Faster R-CNN) for the construction of an end-to-end urine analysis system. We propose an effective baseline for RBCs and WBCs detection on urinary sediment images by using a pre-train Faster R-CNN model. We evaluate our urine analysis system on a large dataset of urinary sediment images which consist of more than 6,000 annotated RBCs and WBCs images. Our results show competitive accuracy and acceptable run time. Prospectively, the proposed methods could provide support to pathology practice in terms of quantitative analysis of tissue constituents in whole-slide images, and it could potentially lead to a better understanding of urinary tract diseases. Code and dataset will be made publicly available.

Keywords- Urinary Sediment; RBC; WBC; Faster R-CNN; Applications in Medicine.

I. INTRODUCTION

Currently, urinary sediment microscopy plays an important role in the clinical diagnosis of urinary tract diseases [1][2]. It is possible to diagnose a patient's disease by identifying the type and amount of sediment in the urine specimen which is effective on early detection and disease control. The development of the Automatic Urinalysis System has been attractive to scholars over the past few years.

The higher clinical value of sediment in the urine mainly includes RBCs and WBCs. The qualitative and quantitative analysis of RBCs and WBCs in urine sediment can not only be helpful in detecting the disease but also help to explore various options for urethral diseases treatment.

Several solutions for urinary sediment microscopy using computer vision methodology have been proposed by different studies [3][4]. However, it is still a challenging task due to the cellular heterogeneity.

In 2005, nephrologists began to report concerns about the frequent discrepancies in some reported results of urine sediment microscopy [5][6]. For instance, the diagnostic accuracy rates of acute kidney injury based on reports by

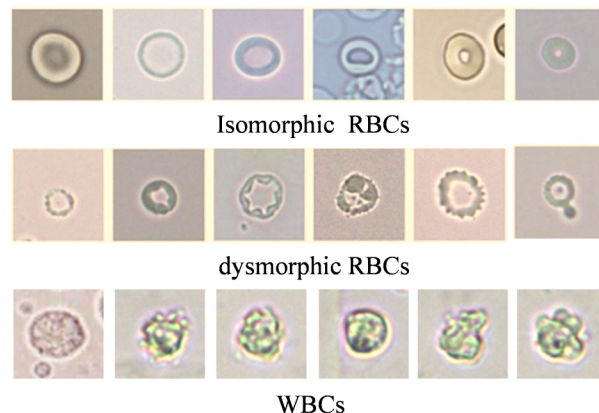


Figure 1. Isomorphic red blood cells (RBCs), dysmorphic RBCs and write blood cells (WBCs).

medical technologists and nephrologists were <25% and 69–92%, respectively [5]. These differences could be caused by the number of dysmorphic red blood cells identified, which tend to be underestimated by image processing technologists. In addition, dysmorphic RBCs were often misclassified as WBCs, besides, the reports issued by medical laboratory technologists overlooked the description of dysmorphic RBCs.

One way to explore these cell types is to use morphological clues in local neighborhoods to develop automated cellular recognition via image analysis, which can then be deployed for sophisticated tissue morphometry.

There are several factors that impede automatic detection and classification of RBCs and WBCs. On one hand, the inferior image quality may arise due to autofocus failure during the digitization of slide. On the other hand, complex tissue architecture, clutter of nuclei, and diversity of nuclear morphology pose a challenging problem.

Particularly, in case of the large numbers of dysmorphic RBCs appearing at urinary sediment, the detection accuracy is significantly declined, due to the dysmorphic RBCs is very similar to the WBCs in terms of cellular morphology (Figure 1). Dysmorphic RBCs are usually transformed by the red blood cells being squeezed through the walls of the blood vessels, causing the damage of cell wall. Furthermore, such cases are not rare. Therefore, we need an effective approach to distinguish the variety of objects from urine sediment, especially isomorphic RBCs, dysmorphic RBCs and WBCs.

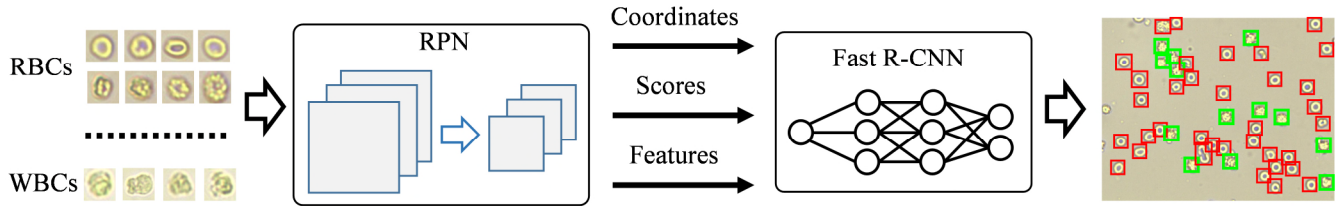


Figure 2. Our urinary sediment detection pipeline.

Faster R-CNN [14] is a particularly successful method for general object detection. It consists of two components: region proposal and estimate object candidates, which is generally considered to be more effective for smaller objects detection. However, there are few studies on the use of Faster R-CNN for urinary sediment detection.

In this paper, we would investigate issues involved Faster R-CNN for construction of end-to-end urine analysis system. In addition, we would propose an effective baseline for RBCs and WBCs detection on urinary sediment images by using a pre-train Faster R-CNN model. In here, we expect both isomorphic RBC and dysmorphic RBC to be detected as RBC.

The rest of the paper is organized as follows: Section 2 introduces the related works. Section 3 presents the pipeline that we used for detecting RBCs and WBCs. Section 4 is devoted to experimental evaluation, whereas conclusions are drawn in Section 5.

II. RELATED WORK

Cell and nucleus classification have been applied to diverse histopathology related applications. Most existing methods for cells detection share similar computation pipelines: thresholding followed by morphological operations, region growing, level sets, k-means, and graph-cuts.

Cosatto et al. [7] proposed the detection of cell nuclei using the difference of Gaussian (DoG) followed by Hough transform to find radially symmetrical shapes. Vink et al. [8] employed AdaBoost classifier to train two detectors, one used pixel-based features and the other merged the results of two detectors to detect the nuclei in immunohistochemistry stained breast tissue images on the base of Haar-like features. Dalle et al. [9] and Cosatto et al. [7] used shape, texture and size of nuclei for nuclear pleomorphism grading in breast cancer images.

Recently, the prevalent success of deep learning approach in computer vision, such as Regions with Convolutional Neural Network (R-CNN) [10], Region Proposal Network & Binary Forest (RPN_BF) [11] and Spatially Constrained Convolutional Neural Network (SC-CNN) [12] have shown good performance on a large number of histopathological image datasets. The R-CNN method [10] trains CNNs end-to-end to classify the proposal regions into object categories or background. Fast R-CNN [13] enables end-to-end detector training on shared convolutional features and shows compelling accuracy and speed. In [11], an RPN_BF approach has been proposed an RPN that

generates candidate boxes, convolutional feature maps, and a Boosted Forest that classifies these proposals using these convolutional features. Korsuk et al. [12] proposed a SC-CNN classifier to detect colon cancer cells.

III. CONVOLUTIONAL NEURAL NETWORK

CNN is one of the basic theories for deep learning, therefore we briefly recap such network.

A CNN f is a composition of a sequence of L functions or layers (f_1, \dots, f_L) that maps an input vector x to an output vector y , i.e.,

$$\begin{aligned} Y &= f(x; w_1, \dots, w_L) \\ &= f_L(\cdot; w_L) \circ f_{L-1}(\cdot; w_{L-1}) \circ \dots \\ &\quad \circ f_2(\cdot; w_2) \circ f_1(\cdot; w_1) \end{aligned} \quad (1)$$

where w_l is the weight and bias vector for the l the layer fl. Conventionally, f_l is defined to perform one of the following operations: a) convolution with a bank of filters; b) spatial pooling; and c) non-linear activation. Given a set of N training data $\{(x^i, y^i)\}_{i=1}^N$, we can estimate the vectors w_1, \dots, w_L by solving the optimization problem

$$\operatorname{argmin}_{w_1, \dots, w_L} \frac{1}{N} \sum_{i=1}^N l(f(x^i; w_1, \dots, w_L), y^i) \quad (2)$$

where l is an appropriately defined loss function. Numerical optimization of (2) is often performed via backpropagation and stochastic gradient descent methods.

IV. RBC AND WBC DETECTION BASED ON FASTER R-CNN

In this section, we describe our RBCs and WBCs detection pipeline for urinary sediment images by Faster R-CNN [14].

Faster R-CNN consists of two components, as shown in Figure 2: an RPN that generates candidate boxes as well as convolutional feature maps, and a Fast R-CNN used for object detection. RPN is used to compute candidate bounding boxes, scores, and convolutional feature maps. The candidate boxes are fed into Fast R-CNN for further classification, using the features pooled from the convolutional feature maps computed by RPN. Finally, non-maximum suppression (NMS) is used to merge the similar results and get the output. In here, we use a urinary sediment image dataset to train the RPN and Fast R-CNN network.

A. RPN network

The RPN network shares full-image convolutional features with the detection network, thus enabling nearly cost-free region proposals. An RPN is a fully convolutional network that simultaneously predicts object bounds and objectness scores at each position. The RPN is trained end-to-end to generate high-quality region proposals, which are used by Fast R-CNN for detection.

We fixed the aspect ratio of anchors (Region Proposal Boxes) [14] as 1:1 (width / height). This is because that we need a square box to mark the positions of the cells. This is unlike the original RPN [14] for detect general object that has anchors of multiple aspect ratios. In order to detect multi-scale RBCs and WBCs, we use anchors of 3 different scales, starting from 20 pixels length of square box side with a scaling stride = 1.2.

Following [14], we adopt the VGG-16 net [15] pre-trained on the ImageNet dataset [16] to initialize the network parameters. The RPN is built on top of the Conv5_3 layer, which is followed by an intermediate 3x3 convolutional layer and two sibling 1x1 convolutional layers for classification and bounding box regression (more details in [14]). The output layer of the RPN net provides confidence scores and regression coordinate of the predicted boxes, which can be used as the input for Fast R-CNN network.

B. Fast R-CNN network

For the detection process, we adopt Fast R-CNN network as mentioned at [14]. To speed up the process, [14] developed a technique that allows for sharing convolutional layers between the two networks, rather than learning two separate networks. For the convenience of the reader, we briefly recap such approach.

A 4-step training algorithm has been adopted to learn shared features via alternating optimization. In the 1st step, the RPN network has been train. And this network is initialized with an ImageNet pre-trained model and fine-tuned end-to-end for the region proposal task. In the 2nd step, they train a separate detection network by Fast R-CNN using the proposals generated by the 1st step. In the 3rd step, they use the detector network to initialize RPN training, but fix the shared convolutional layers and only fine-tune the layers unique to RPN. Finally, keeping the shared convolutional layers fixed, and fine-tune the unique layers of Fast R-CNN. As such, both networks share the same convolutional layers and form the Faster R-CNN network. In this solution, the RPN and Fast R-CNN networks are merged into one network during training.

C. Implementation Details

For RPN and Fast R-CNN training, an anchor is considered as a positive example if it has an Intersection-over-Union (IoU) ratio greater than 0.7 with one ground truth box, and otherwise consider as negative. For Fast R-CNN training, we construct the training set by selecting the top-ranked 100 proposals of each image by RPN network. At test process, we only use the top 300 proposals in an image, which are classified by the Fast R-CNN. We adopt NMS to output the detect results.

V. EXPERIMENT AND RESULTS

In this section, we describe our experimental setup details and the results.

A. The dataset

This study involves electron microscope image. We collected urine samples from 100 patients, and through urine centrifuge to obtain urine sediment. It was then magnified by an electron microscope 400 times and photographed with a digital camera. All images have a common size of 1280 x 1024 pixels.

Manual annotations of nuclei were conducted mostly by an experienced pathologist and partly by a graduate student under supervision of and validation by the same pathologist. A total number of 5,215 RBCs and 4,828 WBCs were

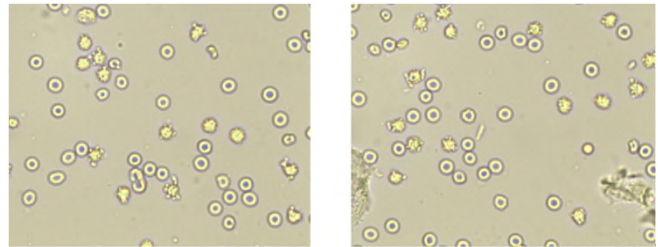


Figure 3. Example images of urinary sediment images dataset used in this experiment.

marked. Figure 3 shows some examples of the urinary sediment images in the dataset. We selected 3,000 random images as the training samples. The test samples also included 2,000 images selected from the rest of the dataset.

B. Evaluation metrics

The objective of this experiment is to detect all RBCs and WBCs in an image by locating their positions, and obtain their class labels. In particular, the performance of an algorithm is evaluated in terms of the tradeoff between precision, Recall, and F1 score.

First, a detected bounding box and a ground truth bounding box (GT) are considered a true positive (TP) if the area covered by their intersection $\geq 70\%$. A GT that does not have a match is considered a False Negative (FN), or a Miss. A detected bounding box that does not have a matching GT is considered as a False Positive (FP). The F1 score (also F-score or F-measure) is a measure of a test's accuracy. It considers both the precision p and the recall r of the test to compute the score: p is the number of correct positive results divided by the number of all positive results, and r is the number of correct positive results divided by the number of positive results that should have been returned. Here, we use F1 score to quantitatively assess the detection performance. The F1 score is computed by the following equation:

$$F_1 = 2 \cdot \frac{precision \cdot recall}{precision + recall} \tag{3}$$

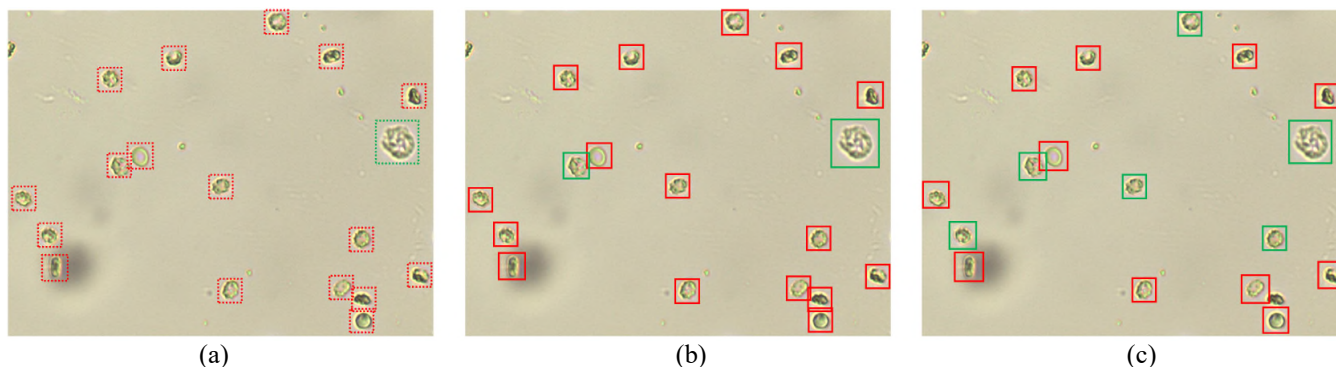


Figure 4. Qualitative results for RBCs and WBCs detection in urine images. (a) Ground truth image. (b) Detection results of our approach. (c) Detection results of RPN_BF.

C. Comparative Results

In this section, our final detectors were evaluated with other state-of-the-art methods using our urinary sediment dataset.

Figure 4 and Table 1 report the performance on detection and classification for our dataset. Figure 4 are qualitative results for RBCs and WBCs detection in urine images. (a) Ground truth image. RBCs are shown as red dashed Box, WBCs are shown as green dashed box. (b) Detection results of our approach. (c) Detection results of RPN_BF. Here, detected as RBCs are shown as red box, and detected as WBCs are shown as green box. It can be seen that our detector show better performance.

TABLE I. COMPARATIVE RESULT FOR RBCS AND WBCS DETECTION

Method	Weighted Average F1 score
Our	0.914
RPN_BF	0.862
HOG	0.688

From the results of the images it can be seen that our detector is competitive in terms of the detection quality with respect to RPN_BF and provides significant improvement over HOG+SVM.

In addition, we have observed the shapes of isomorphic RBCs can change in response to the osmolarity of urine. The isomorphic RBCs swell to spheres in urine with a low specific gravity, and they shrink to the shape of a spiked disk or a spiked sphere in urine with a high specific gravity.

The presence of dysmorphic RBCs leads to the difficulty of distinguishing, which may seriously affects the accuracy of the urinary sediment microscopy system. Therefore, a precise count of dysmorphic RBCs is very important for evaluating glomerular bleeding before renal biopsy.

We profiled the execution of our system on a desktop architecture which features a 2.4GHz Intel i7 CPU, a NVIDIA GTX1080 GPU and 32GB of RAM. The system requires, on average, 96ms to process a frame at a resolution of 1280×1080 pixels. It can be consider as an acceptable running time.

VI. CONCLUSION

In this paper, we investigate issues involving Faster R-CNN for construction of end-to-end urine analysis system. We proposed an effective baseline for RBCs and WBCs detection on urinary sediment images, using a pre-train Faster R-CNN model. Isomorphic, dysmorphic RBCs and WBCs were successfully identified. We comprehensively evaluate this method, the experiment results presenting competitive accuracy and acceptable speed.

Prospectively, the proposed methods could benefit the pathology practice in terms of quantitative analysis of tissue constituents in whole-slide images, and could potentially lead to a better understanding of urinary tract diseases.

However, this study only focused on type 2 cells in urinary sediment, our current results will require additional studies using a wider spectrum of cells and sediment, for examples, Epithelial Cells, Bacteria, Yeast and Parasites. In future work, more theoretical and experimental studies will be conducted to analyze the performance.

REFERENCES

- [1] M. A. Perazella, "The Urine Sediment as a Biomarker of Kidney Disease," American Journal of Kidney Diseases, vol. 66, pp. 748–755, 2015.
- [2] J. A. Simerville, W. C. Maxted, and J. J. Pahira, "Urinalysis: a comprehensive review," American family physician, vol. 71, pp. 1153–1162, 2005.
- [3] M. Yasuda, "Japanese guideline for clinical research of antimicrobial agents on urogenital infections," Journal of Infection and Chemotherapy, vol. 17, pp. 579–594, 2011.
- [4] R. Davis, et al. "Diagnosis, evaluation and follow-up of asymptomatic microhematuria (AMH) in adults," Journal of Urology, vol. 188, pp. 2473–2481, 2012.
- [5] J. J. Tsai, J. Y. Yeun, V. A. Kumar, and B. R. Don, "Comparison and interpretation of urinalysis performed by a nephrologist versus a hospital-based clinical laboratory," American journal of kidney diseases, vol. 46, pp. 820–829, 2005.
- [6] M. Kanbay, B. Kasapoglu, and M. A. Perazella, "Acute tubular necrosis and prerenal acute kidney injury: utility of urine microscopy in their evaluation a systematic review," Int. Urol. Nephrol., vol. 42, pp. 425–433, 2010.

- [7] E. Cosatto, M. Miller, H. P. Graf, and J. S. Meyer, "Grading nuclear pleomorphism on histological micrographs," *Int. Conf. Pattern Recognition*, pp. 1–4, 2008.
- [8] J. P. Vink, M. Van Leeuwen, C. Van Deurzen, and G. De Haan, "Efficient nucleus detector in histopathology images," *Journal of microscopy*, vol.249, no. 2, pp. 124–135, 2013.
- [9] J. R. Dalle, H. Li, C. H. Huang, and W. K. Leow, "Nuclear Pleomorphism Scoring by Selective Cell Nuclei Detection," *IEEE Winter Conf. on Applications of Computer Vision*, pp. 1–6, 2009.
- [10] R. Girshick, J. Donahue, T. Darrell, U. C. Berkeley, J. Malik, "R-CNN: Region-based Convolutional Neural Networks," *Computer Vision and Pattern Recognition*, pp. 2–9, 2014.
- [11] L. Zhang, L. Lin, X. Liang, K. He, "Is Faster R-CNN Doing Well for Pedestrian Detection?" *European Conference on Computer Vision*, pp. 1–15, 2016.
- [12] K. Sirinukunwattana, S.E.A. Raza, Y.W. Tsang, I.A. Cree, D.R.J. Snead, N.M. Rajpoot, "Locality Sensitive Deep Learning for Detection and Classification of Nuclei in Routine Colon Cancer Histology Images," *IEEE Transactions on Medical Imaging*, pp. 1196–1206, 2016.
- [13] R. Girshick, "Fast R-CNN: Fast Region-based Convolutional Networks for object detection," *IEEE International Conference on Computer Vision*, pp. 1440–1448, 2016.
- [14] S. Ren, K. He, R. Girshick, J. Sun, "Faster R-CNN: Towards Real-Time Object Detection with Region Proposal Networks," *Advances in neural information processing systems*, pp. 91–99, 2015.
- [15] L. C. Chen, G. Papandreou, I. Kokkinos, K. Murphy, A. L. Yuille, "Semantic Image Segmentation with Deep Convolutional Nets and Fully Connected CRFs," *International Conference on Learning Representations*, pp. 1–14, 2016.
- [16] O. Russakovsky, et al. "ImageNet Large Scale Visual Recognition Challenge," *International Journal of Computer Vision*, vol. 115, pp. 211–252, 2015.